Critical Role of Perovskite Film Stoichiometry in Determining Solar Cell Operational Stability: a Study on the Effects of Volatile A-Cation Additives

Peer-reviewed author version

SONG, Wenya; XIN, Zhang; LAMMAR, Stijn; Qiu, WM; KUANG, Yinghuan; RUTTENS, Bart; D'HAEN, Jan; Vaesen, I; Conard, T; Abdulraheem, Y; AERNOUTS, Tom; Zhan, YQ & POORTMANS, Jef (2022) Critical Role of Perovskite Film Stoichiometry in Determining Solar Cell Operational Stability: a Study on the Effects of Volatile A-Cation Additives. In: ACS APPLIED MATERIALS & INTERFACES, 14 (24) , p. 27922 -27931.

DOI: 10.1021/acsami.2c05241
Handle: http://hdl.handle.net/1942/40393

Critical role of perovskite film stoichiometry in determining solar cell operational stability: a study on the effects of volatile A-cation additives

Wenya Song[1,2,3,4,#], *Xin Zhang*[1,2,3,4,5,6,#], *Stijn Lammar*[1,2,3,4,#], *Weiming Qiu*[7,*], *Yinghuan Kuang*[2,3,4,*], *Bart Ruttens*[4], *Jan D'Haen*[4], *Inge Vaesen*[7], *Thierry Conard*[7], *Yaser Abdulraheem*[8], *Tom Aernouts*[2,3,4], *Yiqiang Zhan*[5,6], *Jef Poortmans*[1,2,3,4,*]

1. Department of Electrical Engineering (ESAT), Katholieke Universiteit Leuven, Kasteelpark Arenberg 10, 3001 Leuven, Belgium

2. Imec, imo-imomec, Thin Film PV Technology – partner in Solliance, Thor Park 8320, 3600 Genk, Belgium

3. EnergyVille, imo-imomec, Thor Park 8320, 3600 Genk, Belgium

4. Hasselt University, imo-imomec, Martelarenlaan 42, 3500 Hasselt, Belgium

5. Center for Micro Nano Systems, School of Information Science and Technology (SIST), Fudan University, 200433 Shanghai, P. R. China

6. Academy for Engineering & Technology (FAET), Fudan University, 200433 Shanghai, P. R. China

7. imec, Kapeldreef 75, 3001 Leuven, Belgium

8. Department of Electrical Engineering, Kuwait University, 13060 Safat, Kuwait

# These authors contributed equally to this work

Corresponding Author

* Email: Weiming.Qiu@imec.be; Yinghuan.Kuang@imec.be; Jef.Poortmans@imec.be

ABSTRACT

Volatile A-cation halide (AX) additives like formamidinium chloride (FACl) and methylammonium chloride (MACl) have been widely employed for high-efficiency perovskite solar cells (PSCs). However, it remains unstudied how they influence the perovskite film stoichiometry and the solar cell performance and operational stability. Hereby, our work shows that over-annealing of FACl-containing perovskite films leads to a Pb-rich surface, resulting in a high initial efficiency, which however decays during maximum power point tracking (MPPT). On the contrary, perovskite films obtained by a shorter annealing time at the same temperature provide good stability during MPPT but a lower initial efficiency. Thus, we deduce an optimal annealing is vital for both high efficiency and operational stability, which is then confirmed in the case where MACl additive is used. With optimized perovskite annealing condition, we demonstrate efficient and stable p-i-n PSCs that show a best PCE of 20.7% and remain 90% of the initial performance after a 200-hour MPPT at 60 °C under simulated 1-sun illumination with high UV content. Our work presents a comprehensive understanding on how volatile AX impact perovskite film stoichiometry and its correlation to the device performance and operational stability, providing a new guideline for fabricating high-efficiency and operational stable PSCs.

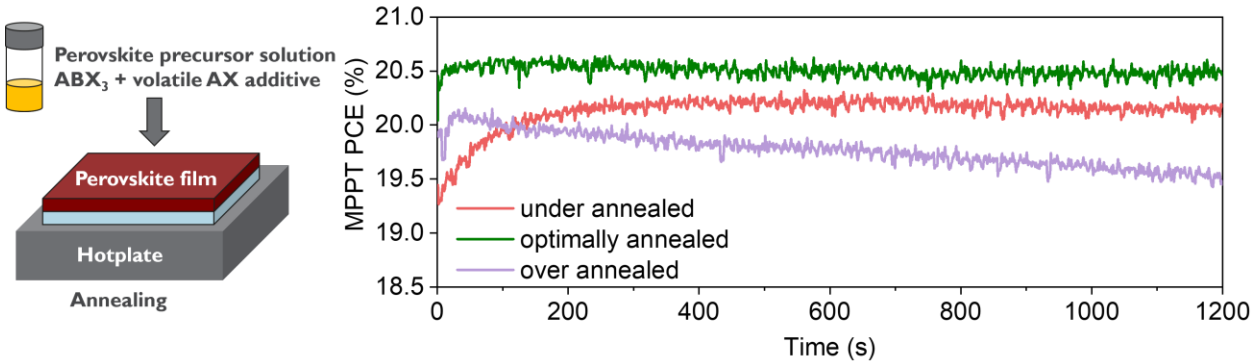

1. INTRODUCTION

Organometal halide perovskite solar cells (PSCs) have achieved more than 25% efficiency[1–4] and their operational stability has also seen significant progress.[5–8] However, the root-causes of device degradation under operation are still not fully understood, which is critical for further improvement of device operational stability. Previous studies have shown that the composition of perovskite films plays a crucial role in determining device stability.[6,9] On the one hand, it is generally believed that methylammonium-free perovskites, e.g. Formamidinium cesium (FACs) cation based perovskites, are better than the ones containing methylammonium cation (MA^+), due to the volatile nature of MA compound that changes the perovskite film stoichiometry.[10,11] On the other hand, volatile additives such as FACl[12–14] and MACl[15–19] have been widely used to achieve high-efficiency perovskite solar cells, since they could optimize the perovskite crystal formation dynamics.[17,20] This brings the scientific question currently scarcely studied, i.e., how such volatile additives influence the perovskite film stoichiometry and how this correlates to the device performance and operational stability.

We first carried out our investigation on the gas-quenched perovskite films with a nominal composition of $Cs_{0.1}FA_{0.9}PbI_{2.865}Br_{0.135}$ which were prepared with volatile FACl as the additive. By changing the thermal annealing time during film process, the stoichiometry of the perovskite film can be well controlled. This enables us to link the film stoichiometry to the device operational stability. Our results show that an optimal annealing condition is crucial to achieve both high efficiency and long-term stability. The over annealing of perovskite film with volatile A-cation additives results in an A-cation deficiency or in other words a Pb-rich surface, which leads to a high initial power conversion efficiency (PCE). However, this kind of high-PCE solar cells degrade fast under the solar cell operational MPPT condition. On the contrary, perovskite

films obtained from less annealing time at the same temperature provide good stability under MPPT but at a lower initial efficiency. The same trend is then further confirmed in the case where MACl is used as the additive. With careful control on the thermal annealing condition, we demonstrate efficient and stable PSCs that show a best PCE of 20.7% and remain 90% of the initial performance after MPPT tracking for 200 hours at 60 °C under 1 sun illumination with high UV content. Our work presents a comprehensive understanding on the role of volatile additives on the perovskite film stoichiometry and its correlation to the device performance and operational stability, providing a new guideline for the fabrication of high-efficiency and operational stable PSCs.

2. RESULTS AND DISCUSSION

2.1 Stoichiometry control of perovskite films

In this study, we employed the dual-cation perovskite films with a nominal ABX_3 composition of $Cs_{0.1}FA_{0.9}PbI_{2.865}Br_{0.135}$ on glass/ITO/poly[bis(4-phenyl) (2,4,6-trimethylphenyl) amine] (PTAA) substrates, fabricated from a gas-quenching method shown in **Figure 1**. The perovskite films with volatile FACl additive were prepared from the precursor solution with 5 mol% excess FACl compared to the stoichiometric ABX_3 composition (denoted as ABX_3 + 5% excess FACl). To investigate the influence of thermal annealing condition on perovskite stoichiometry, we annealed the as-prepared films made from the same solution at 130 °C for 1, 5, 10, 20, 30 and 40 min in a N_2-filled glovebox, respectively. Furthermore, two reference films are prepared respectively from stoichiometric precursor solution without any additive (denoted as ABX_3) and with 3.17 mol% extra $PbCl_2$ (denoted as ABX_3 + 3.17% excess $PbCl_2$). The reference films were both annealed at 130 °C for 10 min. This way, we covered precursor solution formulars from

ABX_3 + excess AX to stoichiometric ABX_3, and further to ABX_3 + excess BX_2. Scanning electron microscopy (SEM), X-ray diffraction (XRD), X-ray photoelectron spectroscopy (XPS) and photoluminescence (PL) were carried out to examine morphology, crystallinity, and stoichiometry of the films.

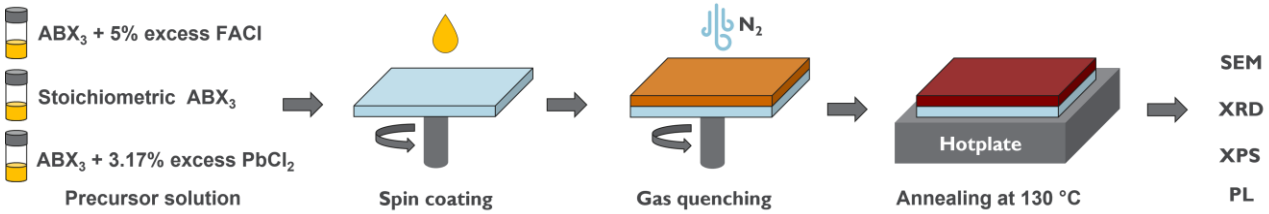

Figure 1. Schematic representation of the processing procedures of perovskite films and the characterizations performed on the films.

Figure 2 shows the secondary electron (SE) SEM images of the eight films mentioned above. Plate-like phases are present on stoichiometric and 3.17% excess $PbCl_2$ films (**Figure 2 (g, h)**). Positions of these plate-like phases correspond to bright phases in Inlens SEM images (**Figure S1 and Figure S2 (g, h)**). According to previous studies, such bright phases often represent PbI_2.[21–24] On the contrary, the plate-like phases are absent in all the films prepared with 5% excess FACl solution and annealed for 1 – 40 min (**Figure 2 (a-f)**). However, it is noticeable that as the annealing time increases, the surface morphology of 5% excess FACl films changes. The 5% excess FACl 30 min film started to show fringes on perovskite grains (**Figure 2 (e)**). Flat grain surfaces appeared on the 5% excess FACl 40 min film (**Figure 2 (f)**).

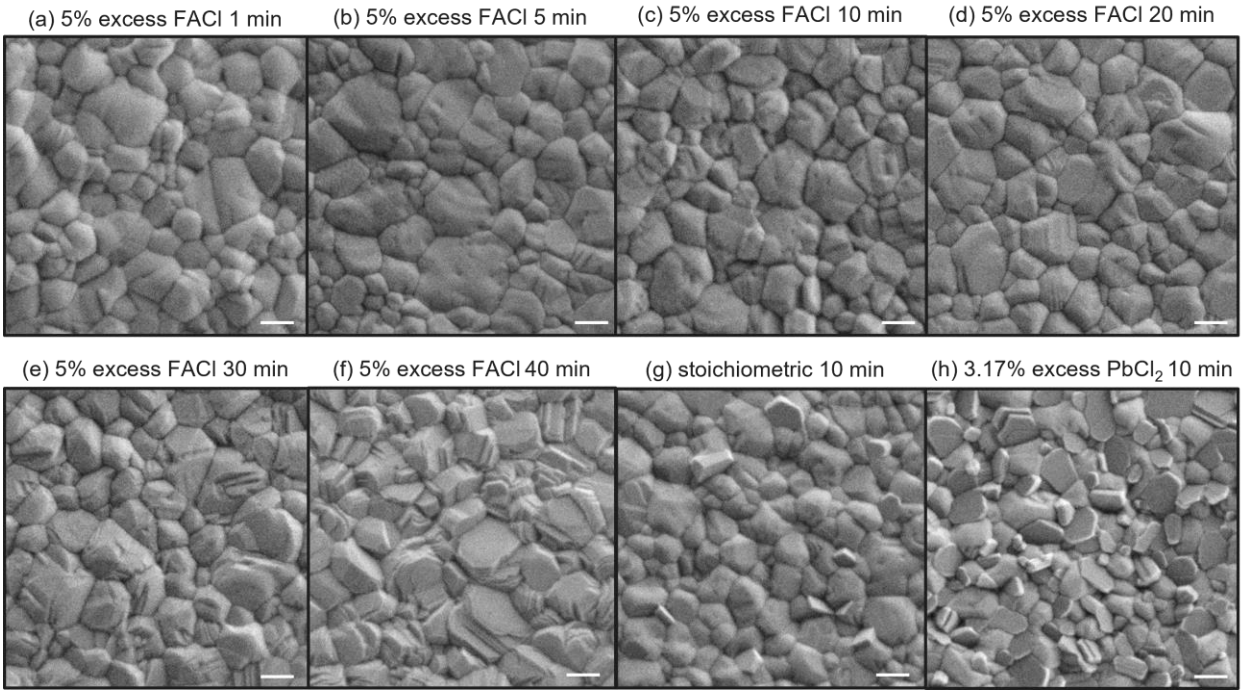

Figure 2. (a-h) Secondary electron mode SEM images of the corresponding perovskite films. The length of the scale bars indicates 200 nm.

Figure 3 (a) shows the XRD patterns of these eight films. All the films show main diffraction peaks at 14.0°, 28.3°, and 31.7°, indicating the (001), (002), and (012) planes of cubic phase perovskite.[25–28] The stoichiometric 10 min film and the 3.17% excess $PbCl_2$ film both show diffraction peaks at 12.7°, which is classified as the (001) peak in cubic phase PbI_2.[29–31] The PbI_2 peak intensity in the stoichiometric 10 min film is less than that of the 3.17% excess $PbCl_2$ 10 min film, just as the flake amount in the stoichiometric 10 min film is less than that in the 3.17% excess $PbCl_2$ film. In the meantime, the $PbBr_2$ and $PbCl_2$ characteristic XRD peaks are not observed.[29] Thus, we can safely deduce the plate-like phases in **Figure 2 (g, h)** are PbI_2.

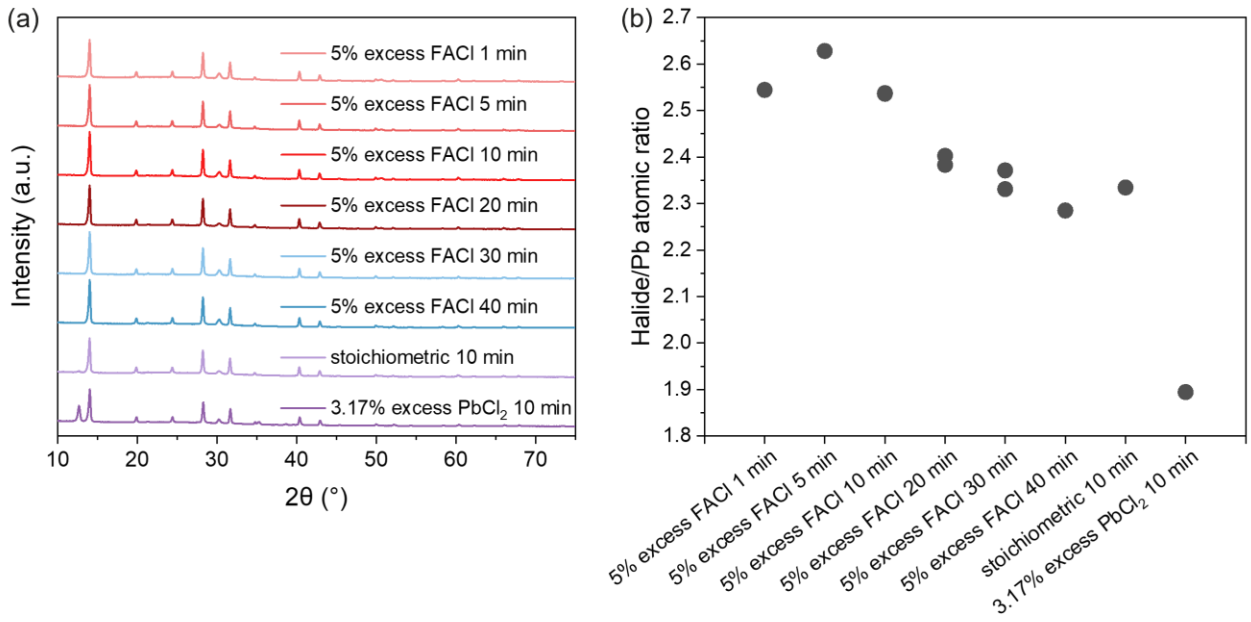

Figure 3. (a) XRD patterns and (b) Halide/Pb atomic ratios from XPS measurements of the eight types of perovskite films. Two films from 5% excess FACl 10 min, 20 min and 30 min conditions were measured, respectively. These data points illustrate reproducibility in XPS measurement. To note, the two data points for 5% excess FACl 10 min films completely overlap.

Figure 3 (b) shows the halide/Pb atomic ratio calculated from XPS measurements. The total halide amount sums the amount of iodide, bromide, and chloride. The Pb amount sums the amount of both Pb^{2+} and metallic Pb. The $4f_{7/2}$ Pb signals from XPS measurements of each perovskite films are shown in **Figure S3**, where the peaks at 138.4 eV originates from Pb^{2+}, and the peaks at 136.6 eV are associated with metallic Pb.[32] According to precedent studies,[11,33,34] the metallic Pb is detected due to the photolysis of PbX_2 into Pb and X_2 under X-ray. To note, under X-ray irradiation, ABX_3 perovskite also decomposes into PbX_2, which can further decompose to Pb.[33] Thus, it is reasonable that the halide/Pb ratio of perovskite surface is lower than 3. As we can see from **Figure 3 (b)**, the 3.17% excess $PbCl_2$ 10 min film shows the lowest halide/Pb ratio

of 1.89 among all the films, suggesting this film has a large amount of PbX_2 at the surface. The stoichiometric 10 min film shows a halide/Pb ratio of 2.33, implying the surface of this film is a mixture of ABX_3 perovskite and PbX_2 and it has less PbX_2 compared to that in the 3.17% excess $PbCl_2$ 10 min film. These observations well align with those in SEM and XRD shown in **Figure 2 (g, h)** and **Figure 3 (a)**. We can observe a trend that as the annealing time of the 5% excess FACl films increases from 1 min to 40 min, the halide/Pb ratio decreases from the highest point of 2.63 to lowest point of 2.29. Despite the decreasing halide/Pb ratio, none of the 5% excess FACl films show PbI_2 signals in XRD spectrum (**Figure 3 (a)**), indicating PbI_2 crystals are not formed. However, the SEM images **Figure 2 (a-f)** show that as the annealing time increases, the perovskite grain surface starts to show fringes and become flat. Thus, we can deduce a Pb-rich perovskite crystal facet is likely formed as the annealing time of 5% excess FACl film increases, which leads to a low halide/Pb ratio at the surface.

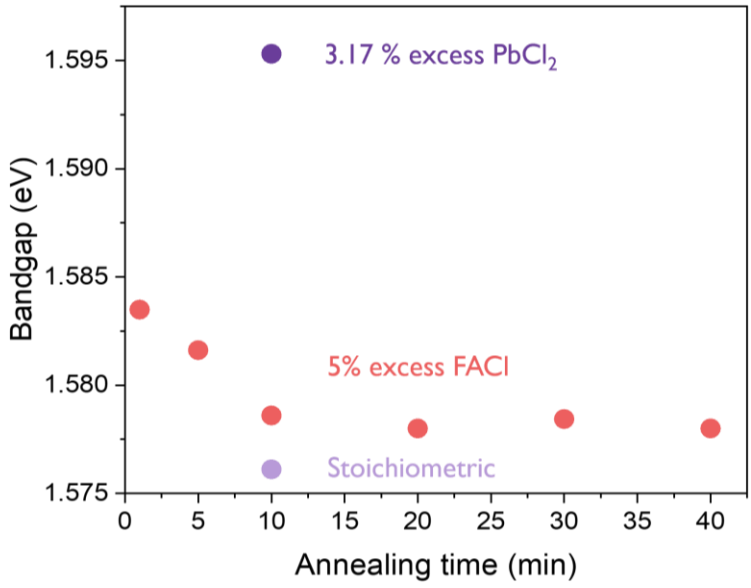

Figure 4. Bandgap of the eight investigated perovskite films calculated from steady-state photoluminescence.

Apart from deducing surface stoichiometry through a combination of SEM, XRD and XPS, we also deduce the perovskite bulk stoichiometry from bandgap obtained from steady-state photoluminescence (SSPL). **Figure 4** shows the bandgap of stoichiometric 10 min and 3.17% excess $PbCl_2$ 10 min perovskite films are 1.576 eV and 1.595 eV, respectively. The bandgap of 5% excess FACl films first decreases from 1.583 eV to 1.578 eV as the annealing time increases from 1 min to 10 min, then the bandgap stabilizes around 1.578 eV as the annealing time increases from 10 min to 40 min. This trend suggests that in the beginning of annealing, most Cl is still incorporated in the perovskite crystals, leading to a high bandgap.[35] As annealing time increases to 10 min, the amount of Cl in perovskites gradually reduces due to the evaporation of Cl-containing volatile species, leading the bandgap to decrease. Once the Cl amount stabilizes in the perovskite film, the bandgap of the film also stabilizes. We can deduce that once the annealing time exceeds 10 min the bulk stoichiometry likely remains unchanged.

Combining the SEM, XRD, XPS and PL results, we can conclude that during the first 10 min of annealing at 130 °C, the bulk stoichiometry of the 5% excess FACl film changes. When the annealing time exceeds 10 min, the bulk stoichiometry of perovskite films stays unchanged, while the surface of perovskite becomes more Pb-rich. Hence, we can further conclude it's possible to control the bulk and surface stoichiometry of perovskite films with volatile AX excess through simply controlling their annealing time.

2.2 Linking perovskite film stoichiometry with solar cell operational stability.

To unveil the relation between perovskite stoichiometry and solar cell operational stability, we fabricated solar cells with the structure of glass/ITO/PTAA/perovskite/C_{60}/BCP/Cu (**Figure 5 (a)**), where perovskite layers are the eight types of films investigated in the previous section. The

initial PCEs obtained from *J-V* scans in **Figure 5 (b)** show that as the annealing time of 5% excess FACl perovskites increase from 1 min to 40 min, the average initial PCE first increases from 5.5 % (1 min) to 18.3% (30 min) and then drops to 17.8% (40 min). The average initial PCE of stoichiometric 10 min and 3.17% excess $PbCl_2$ 10 min perovskites are 15.6% and 18.4%, respectively. The rest parameters from *J-V* scans are presented in **Figure S4**.

Interestingly, despite the higher initial PCE, the 3.17% excess $PbCl_2$ 10 min, stoichiometric 10 min, 5% excess FACl 40 min and 30 min PSCs all show declining PCE during the 20-min MPPT under 1-sun illumination from a xenon lamp (**Figure 5 (c)**). In contrast, though the 5% excess FACl 1, 5, 10, 20 min PSCs show low initial PCE, during the 20-min MPPT their PCEs keep increasing and eventually stabilize at a higher PCE. For instance, the 3.17% excess $PbCl_2$ 10 min PSC shows a high initial PCE of 18.6%. After 20-min MPPT, its PCE drops to 17.4%. The PCE of 5% excess FACl 30 min PSC is initially 18.5% and it drops to 17.9% at the end of MPPT. On the contrary, the 5% excess FACl 20 min PSC shows a lower initial PCE of 17.2%. Its PCE keeps increasing to 19% in the first 10-minute MPPT, and then stabilizes at 19% till the end. The calculated average PCE of 3.17% excess $PbCl_2$ 10 min, 5% excess FACl 30 min and 5% excess FACl 20 min PSCs during the 20-minute MPPT is 18.0%, 18.0% and 18.7%, respectively. Thus, despite the lower initial PCE from the 5% excess FACl PSC, it generates more energy in 20 minutes than the other two PSCs.

It appears that the perovskite films with Pb-rich surface result in declining PCE during MPPT, while the films with less Pb-rich surface lead to more stable PSCs during MPPT. To verify this discovery in longer term solar cell operation and at harsher conditions, we tracked the MPP of PSCs under 1-sun illumination from metal halide lamp with strong UV for 40 hours. During this tracking, the cell temperatures reached 60 °C. As can be seen from **Figure 5 (d)**, the

stoichiometric 10 min and 3.17% excess $PbCl_2$ 10 min PSCs maintains less than 78% initial PCE. In contrast, the 5% excess FACl 10 min and 20 min PSCs are much more stable, maintaining more than 91% initial PCE at the end of 40-hour MPPT.

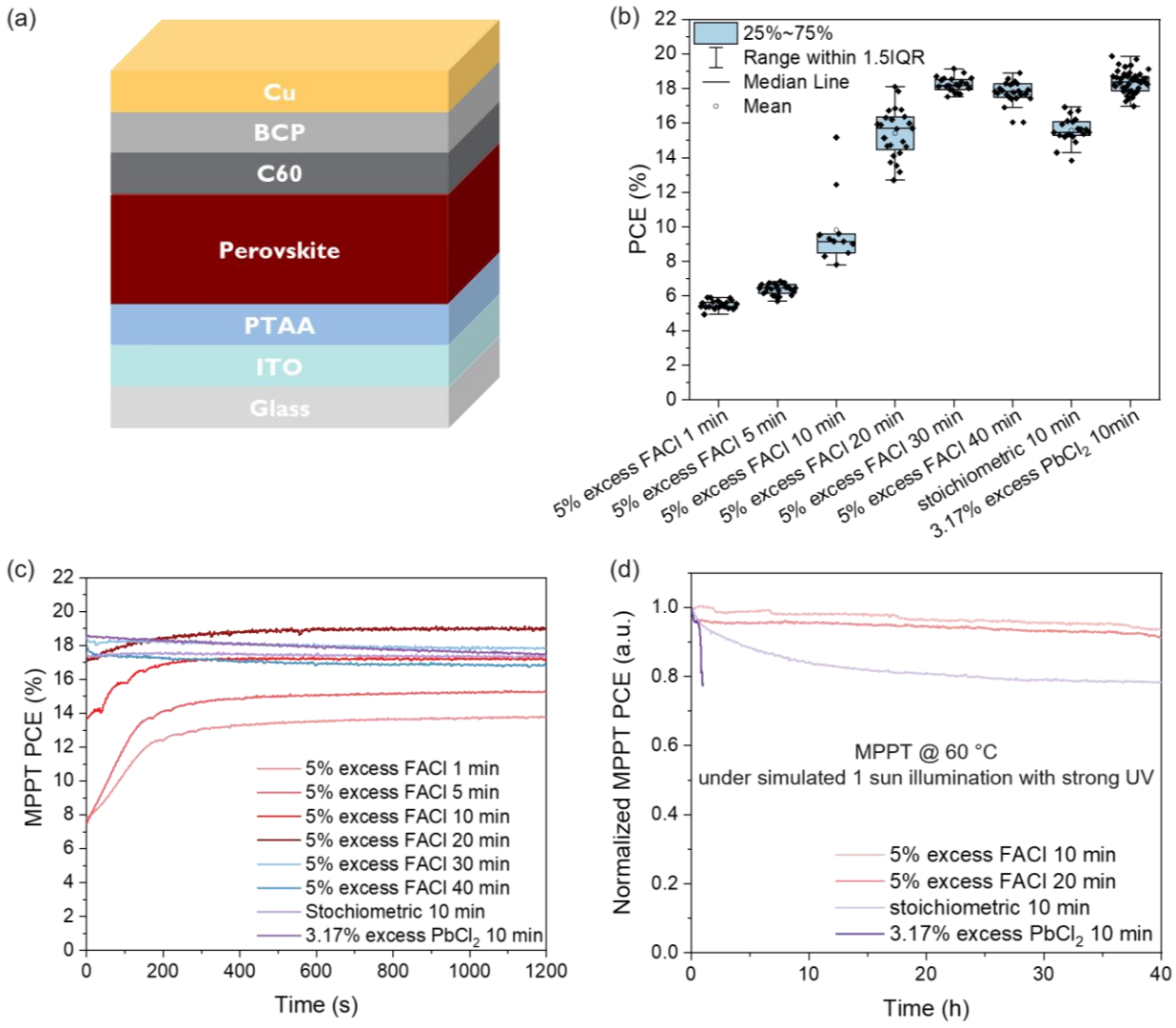

Figure 5. (a) Schematics of the PSC structure. (b) Initial PCE distribution of PSCs with corresponding perovskites films. (c) 20-minute MPPT of PSCs under 1-sun xenon lamp at 30 °C. (d) 40-hour MPPT of corresponding PSCs under simulated 1 sun illumination from a metal halide lamp, which contains strong UV content. The cell temperature reaches 60 °C.

To further prove the above link between perovskite surface stoichiometry and the solar cell operational stability, we performed controlled experiments by changing annealing temperature, annealing time, AX species, and AX amount, then tracking their PCE during MPPT. First, we kept the FACl 5% excess and annealed it at 150 °C instead of 130 °C for 10 min to accelerate the FACl evaporation during annealing. This way, the surface of 5% excess FACl 150 °C 10 min perovskite film will be more Pb-rich than the 5% excess FACl 130 °C 10 min film. As a result, the 150 °C 10 min film indeed shows declining PCE as indicated by the purple curve in **Figure 6 (a)**. Then we drastically increased the amount of FACl excess from 5 % to 30% so that even at the end of a long time annealing the FACl is not able to fully escape the films, potentially creating AX-rich perovskite films. Indeed, after annealing at 130 °C for 80 min, the PSC with this perovskite shows increasing PCE during MPPT as indicated by the blue curve in **Figure 6 (a)**.

To follow up, we then replaced FACl additive with less volatile FAI additive. As is also shown in **Figure 6 (a)**, with a limited amount of 1.5% excess FAI, the device behaves like the denoted stochiometric device, for which the PCE degrades under MPPT tracking. Nevertheless, with the amount of excess FAI increasing to 2.5% and 5%, the devices start to show the opposite trend under MPPT tracking, i.e., PCE first significantly increases and then stabilizes with tracking time. Interestingly, due to the much less volatile nature of FAI than FACl, the annealing time plays a marginal role in the case of FAI additive. In **Figure S5**, nearly identical initial PCEs and MPPT tracking behavior have been observed for the PSCs made with 5% excess FAI but annealed at 130 °C for 20 min, 40 min, 60 min, respectively. Their PCEs all rise in the same fashion from below 2% to above 10% at the end of 20-minute MPPT. The above controlled

experiments clearly prove that despite of low initial PCE, the AX-rich devices are more stable under MPPT.

Finally, we designed another experiment where the 5% excess FACl perovskite film was first annealed at 130 ° C for 60 min to realize a Pb-rich surface. After this, we applied surface treatment on such films by spin coating FAI solutions with different concentrations. **Figure 6 (b)** shows that the 5% excess FACl 130 °C 60 min PSC presents typical declining MPPT PCE. However, as the FAI solution concentration of the surface treatment increases, the perovskite film shall turn from Pb-rich to less Pb-rich and eventually to AX-rich.[24] Correspondingly, **Figure 6 (b)** shows that the devices turn from having the declining MPPT PCE (pristine) to a more stable MPPT PCE (0.5 mg/ml) and then an increasing MPPT PCE (1.0 mg/ml).

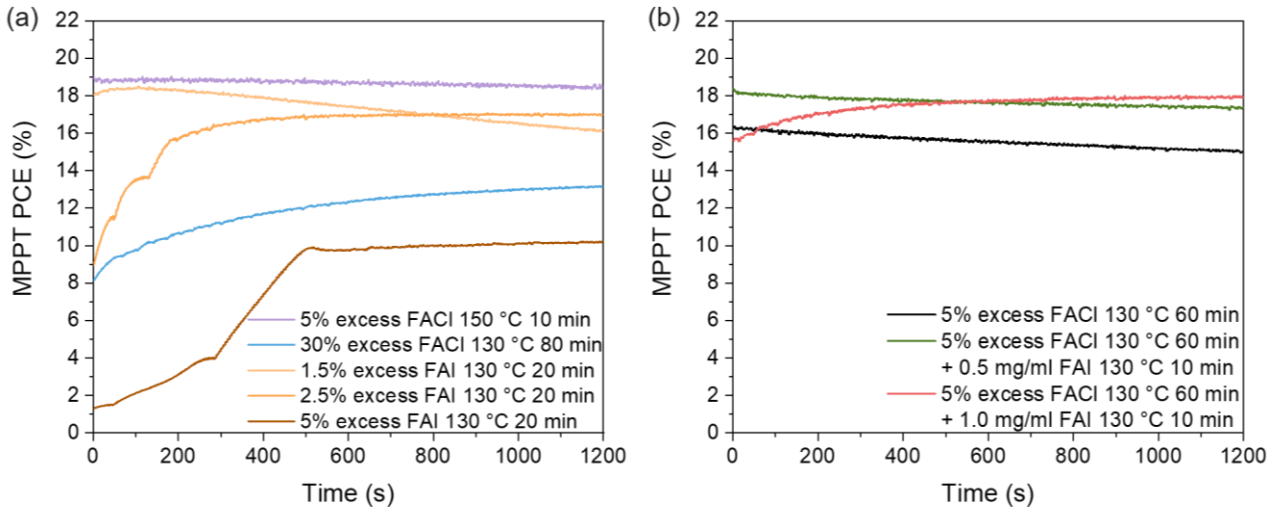

Figure 6. (a) 20-min MPPT of PSCs with corresponding processing conditions. (b) 20-min MPPT of PSCs with and without FAI surface treatment.

To conclude, with the experimental results presented in this section, we can find a clear link between the perovskite film stoichiometry and the solar cell operational stability. Perovskites with Pb-rich surfaces result in high initial PCE but declining PCE during MPPT, while AX-rich

perovskites lead to low initial PCE but increasing MPPT. Therefore, to be able to deliver both high initial PCE and stable MPPT PCE, a careful screening of annealing condition including temperature and duration is needed when the volatile additive is present in the perovskite solution.

2.3 Verify the generality using PSCs with MACl additive

MACl is another commonly used additive for high-efficiency PSCs.[15–19] In order to verify the generality of the above-observed link between stoichiometry and device performance, we have done another case study, where 30 mol% MACl is used as the volatile AX additive in the perovskite precursor solution. The obtained perovskite precursor films were annealed at 110 °C for 50 min, 60 min, 70 min and 80 min, respectively. **Figure 7 (a)** shows the top-view SEM image of the perovskite with MACl additive that was annealed for 60 min. Compared to the one with FACl additive, much larger grain size is realized with MACl additive, which could be attributed to higher amount of chlorine used.[17] The device performance of the gas quenched inverted p-i-n PSCs was evaluated with a configuration of ITO/PTAA/perovskite/LiF/C_{60}/BCP/Cu. The PCE distribution diagram is shown in **Figure 7 (b)** and the other parameters are shown in **Figure S6**. Interestingly, the average PCEs of the devices do not vary significantly with perovskite annealing time, though the devices prepared with films annealed for 60 min show a slightly higher average PCE. However, as displayed in **Figure 7 (c)**, we can find the same link between the annealing time and MPPT behavior as what is shown in the case of perovskite films fabricated with FACl additive. When the perovskite film is annealed for a relatively short time, i.e. 50 min, the corresponding device's MPPT PCE takes about 5 min to increase from the initial 19.3% to a stabilized 20.1%. When an optimal annealing time is applied, i.e. 60 min, we can obtain the highest and the most stable MPPT PCE of 20.5% during

the 20 min tracking time. Once the perovskite film is over annealed, i.e, in the case of 70 min and 80 min, the MPPT PCE keep decreasing during the measurement. In particular, the longer the annealing time is, the more remarkable decrease in MPPT PCE is observed. Similar to the case of FACl, a prolonged annealing time will result in perovskite films with Pb-rich surface since MACl is even more volatile. As discussed above, it is important to carefully control the annealing temperature and duration to achieve high and stable MPPT PCEs. By annealing the precursor films with MACl additive at 110 °C for 60 min, we can achieve the best device performance with negligible hysteresis (**Figure 7 (d)**), and high EQE that leads to an integrated Jsc of 23.3 mA cm^{-2} (**Figure 7 (e)**). More importantly, the device can maintain approximately 90% of the initial performance after 200-hour MPPT at 60 °C under 1 sun illumination from a metal halide lamp with strong UV.

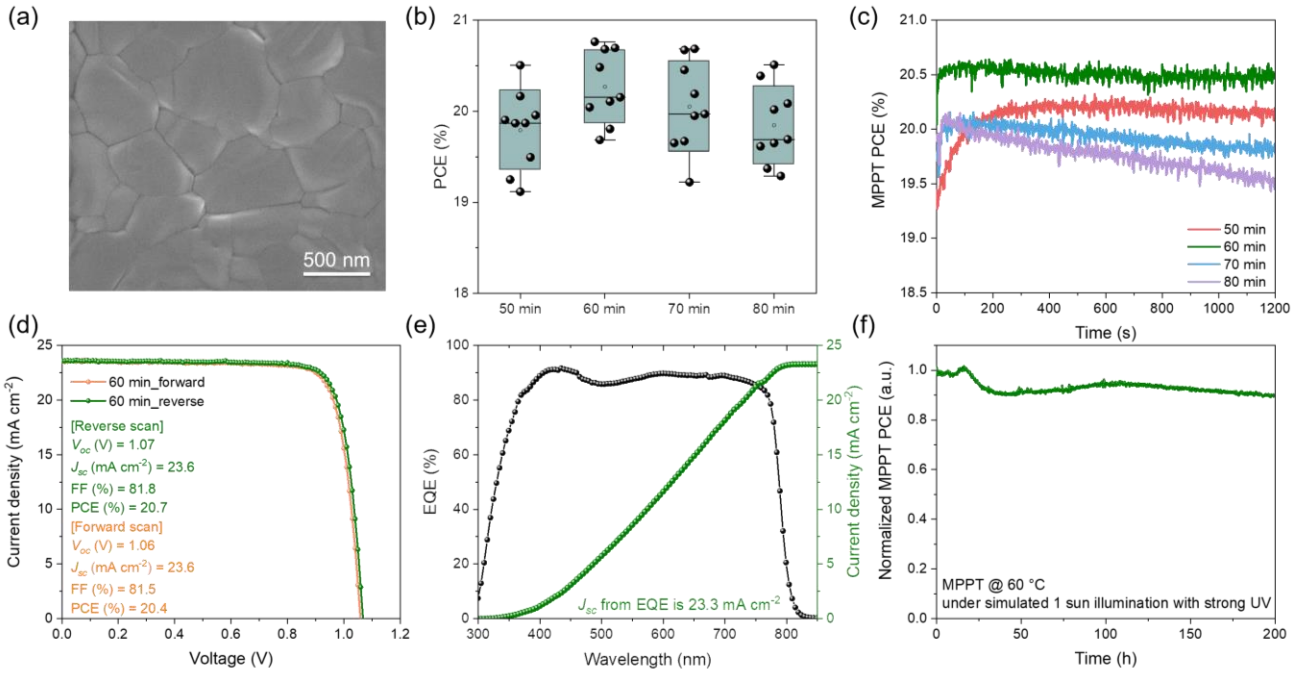

Figure 7. High-efficiency PSCs with 30% MACl additive. (a) Top-view SEM image of the perovskite film. The perovskite film was annealed at 110 °C for 60 min. (b) PCE distribution

diagram of the corresponding gas-quenched PSCs with different perovskite annealing time, including 50 min, 60 min, 70 min and 80 min. (c) 20 min MPPT measurements of the corresponding PSCs. (d) *J-V* curves of the champion device under reverse and forward scans. The inset shows the corresponding PV parameters. (e) EQE and integrated J_{sc} spectra of the champion device. (f) The operational stability test of the PSC based on the optimal condition. The test is carried under simulated 1 sun illumination from a metal halide lamp with strong UV. The cell temperature reaches 60 °C.

CONCLUSION

To conclude, our work reveals the stoichiometry of perovskite films that contain volatile AX additives can be readily controlled by changing their thermal annealing temperature and time. We then unraveled how such volatile additives can influence the perovskite film stoichiometry and how this correlate to the device performance and operational stability. It is discovered that the over annealed perovskite films become Pb-rich at the surface, leading to PSCs with high initial PCE but poor stability under MPPT condition. On the contrary, the under annealed films lead to PSCs with low initial PCEs, but the PCEs increase during MPPT. We verified the generality of this by studying perovskite precursors using either FACl or MACl as an additive, showing it is important to control the annealing conditions to simultaneously achieve the high efficiency and operational stability. With optimally annealed perovskite films, we demonstrate efficient and stable p-i-n PSCs that show the best PCE of 20.7% and remain 90% of the initial performance after a 200-hour MPPT at 60 °C under 1 sun illumination with high UV content. Therefore, this work provides a new guideline for the fabrication of high-efficiency and operational stable PSCs.

ACKNOWLEDGMENT

This work is funded in part by the Kuwait Foundation for the Advancement of Sciences under project numbers CN18-15EE-01 and PN1734SC02. W.Q. would like to thank the financial support of the postdoctoral fellowship grant from Research Foundation-Flanders (FWO Grant No. 1252322N). Y.K. and T.A. acknowledge the funding from the European Union's Horizon 2020 research and innovation program under grant agreement No. 850937 of the PERCISTAND project, and the FLAG-ERA JTC 2019 program under Reference Number of JTC-2019-013 of the LASERGRAPH project.

SUPPORTING INFORMATION

Materials, solution preparation, device fabrication and characterization methods, and supporting data can be found in supporting information document.

REFERENCES

(1) NREL. Best Research-Cell Efficiencies https://www.nrel.gov/pv/assets/pdfs/best-research-cell-efficiencies-rev210726.pdf.

(2) Jeong, J.; Kim, M.; Seo, J.; Lu, H.; Ahlawat, P.; Mishra, A.; Yang, Y.; Hope, M. A.; Eickemeyer, F. T.; Kim, M.; et al. Pseudo-Halide Anion Engineering for α-FAPbI3 Perovskite Solar Cells. *Nature* **2021**, *592* (7854), 381–385. https://doi.org/10.1038/s41586-021-03406-5.

(3) Min, H.; Lee, D. Y.; Kim, J.; Kim, G.; Lee, K. S.; Kim, J.; Paik, M. J.; Kim, Y. K.; Kim, K. S.; Kim, M. G.; et al. Perovskite Solar Cells with Atomically Coherent Interlayers on SnO2 Electrodes. *Nature* **2021**, *598* (7881), 444–450. https://doi.org/10.1038/s41586-021-03964-8.

(4) Yoo, J. J.; Seo, G.; Chua, M. R.; Park, T. G.; Lu, Y.; Rotermund, F.; Kim, Y. K.; Moon, C. S.; Jeon, N. J.; Correa-Baena, J. P.; et al. Efficient Perovskite Solar Cells via Improved Carrier Management. *Nature* **2021**, *590* (7847), 587–593. https://doi.org/10.1038/s41586-021-03285-w.

(5) Li, N.; Niu, X.; Li, L.; Wang, H.; Huang, Z.; Zhang, Y.; Chen, Y.; Zhang, X.; Zhu, C.; Zai, H.; et al. Liquid Medium Annealing for Fabricating Durable Perovskite Solar Cells with Improved Reproducibility. *Science* **2021**, *373* (6554), 561–567. https://doi.org/10.1126/science.abh3884.

(6) Deng, Y.; Xu, S.; Chen, S.; Xiao, X.; Zhao, J.; Huang, J. Defect Compensation in Formamidinium–Caesium Perovskites for Highly Efficient Solar Mini-Modules with

Improved Photostability. *Nat. Energy* **2021**. https://doi.org/10.1038/s41560-021-00831-8.

(7) Li, N.; Tao, S.; Chen, Y.; Niu, X.; Onwudinanti, C. K.; Hu, C.; Qiu, Z.; Xu, Z.; Zheng, G.; Wang, L.; et al. Cation and Anion Immobilization through Chemical Bonding Enhancement with Fluorides for Stable Halide Perovskite Solar Cells. *Nat. Energy* **2019**, *4* (5), 408–415. https://doi.org/10.1038/s41560-019-0382-6.

(8) Wang, L.; Zhou, H.; Hu, J.; Huang, B.; Sun, M.; Dong, B.; Zheng, G.; Huang, Y.; Chen, Y.; Li, L.; et al. A Eu 3+ -Eu 2+ Ion Redox Shuttle Imparts Operational Durability to Pb-I Perovskite Solar Cells. *Science* **2019**, *363* (6424), 265–270. https://doi.org/10.1126/science.aau5701.

(9) Fassl, P.; Lami, V.; Bausch, A.; Wang, Z.; Klug, M. T.; Snaith, H. J.; Vaynzof, Y. Fractional Deviations in Precursor Stoichiometry Dictate the Properties, Performance and Stability of Perovskite Photovoltaic Devices. *Energy Environ. Sci.* **2018**, *11* (12), 3380–3391. https://doi.org/10.1039/c8ee01136b.

(10) Juarez-Perez, E. J.; Hawash, Z.; Raga, S. R.; Ono, L. K.; Qi, Y. Thermal Degradation of CH3NH3PbI3 Perovskite into NH3 and CH3I Gases Observed by Coupled Thermogravimetry-Mass Spectrometry Analysis. *Energy Environ. Sci.* **2016**, *9* (11), 3406–3410. https://doi.org/10.1039/c6ee02016j.

(11) Juarez-Perez, E. J.; Ono, L. K.; Maeda, M.; Jiang, Y.; Hawash, Z.; Qi, Y. Photodecomposition and Thermal Decomposition in Methylammonium Halide Lead Perovskites and Inferred Design Principles to Increase Photovoltaic Device Stability. *J. Mater. Chem. A* **2018**, *6* (20), 9604–9612. https://doi.org/10.1039/c8ta03501f.

(12) Tavakoli, M. M.; Yadav, P.; Prochowicz, D.; Sponseller, M.; Osherov, A.; Bulović, V.; Kong, J. Controllable Perovskite Crystallization via Antisolvent Technique Using Chloride Additives for Highly Efficient Planar Perovskite Solar Cells. *Adv. Energy Mater.* **2019**, *9* (17), 1–10. https://doi.org/10.1002/aenm.201803587.

(13) Dagar, J.; Fenske, M.; Al-Ashouri, A.; Schultz, C.; Li, B.; Köbler, H.; Munir, R.; Parmasivam, G.; Li, J.; Levine, I.; et al. Compositional and Interfacial Engineering Yield High-Performance and Stable p-i-n Perovskite Solar Cells and Mini-Modules. *ACS Appl. Mater. Interfaces* **2021**, *13* (11), 13022–13033. https://doi.org/10.1021/acsami.0c17893.

(14) Prochowicz, D.; Runjhun, R.; Tavakoli, M. M.; Yadav, P.; Saski, M.; Alanazi, A. Q.; Kubicki, D. J.; Kaszkur, Z.; Zakeeruddin, S. M.; Lewiński, J.; et al. Engineering of Perovskite Materials Based on Formamidinium and Cesium Hybridization for High-Efficiency Solar Cells. *Chem. Mater.* **2019**, *31* (5), 1620–1627. https://doi.org/10.1021/acs.chemmater.8b04871.

(15) Kim, M.; Kim, G. H.; Lee, T. K.; Choi, I. W.; Choi, H. W.; Jo, Y.; Yoon, Y. J.; Kim, J. W.; Lee, J.; Huh, D.; et al. Methylammonium Chloride Induces Intermediate Phase Stabilization for Efficient Perovskite Solar Cells. *Joule* **2019**, *3* (9), 2179–2192. https://doi.org/10.1016/j.joule.2019.06.014.

(16) Mateen, M.; Arain, Z.; Yang, Y.; Liu, X.; Ma, S.; Liu, C.; Ding, Y.; Ding, X.; Cai, M.; Dai, S. MACl-Induced Intermediate Engineering for High-Performance Mixed-Cation Perovskite Solar Cells. *Cite This ACS Appl. Mater. Interfaces* **2020**, *12*, 10535–10543. https://doi.org/10.1021/acsami.9b22719.

(17) Odysseas Kosmatos, K.; Theofylaktos, L.; Giannakaki, E.; Deligiannis, D.; Konstantakou,

M.; Stergiopoulos, T. Methylammonium Chloride: A Key Additive for Highly Efficient, Stable, and Up-Scalable Perovskite Solar Cells. *Energy Environ. Mater.* **2019**, *2* (2), 79–92. https://doi.org/10.1002/EEM2.12040.

(18) Gutierrez-Partida, E.; Hempel, H.; Caicedo-Dávila, S.; Raoufi, M.; Peña-Camargo, F.; Grischek, M.; Gunder, R.; Diekmann, J.; Caprioglio, P.; Brinkmann, K. O.; et al. Large-Grain Double Cation Perovskites with 18 Ms Lifetime and High Luminescence Yield for Efficient Inverted Perovskite Solar Cells. *ACS Energy Lett.* **2021**, *6* (3), 1045–1054. https://doi.org/10.1021/acsenergylett.0c02642.

(19) Xiong, Z.; Lan, L.; Wang, Y.; Lu, C.; Qin, S.; Chen, S.; Zhou, L.; Zhu, C.; Li, S.; Meng, L.; et al. Multifunctional Polymer Framework Modified SnO2Enabling a Photostable α-FAPbI3Perovskite Solar Cell with Efficiency Exceeding 23%. *ACS Energy Lett.* **2021**, *6* (11), 3824–3830. https://doi.org/10.1021/acsenergylett.1c01763.

(20) Liang Tan, W.; Yee Choo, Y.; Huang, W.; Jiao, X.; Lu, J.; Cheng, Y.-B.; McNeill, C. R. Oriented Attachment as the Mechanism for Microstructure Evolution in Chloride-Derived Hybrid Perovskite Thin Films. *ACS Appl. Mater. Interfaces* **2019**, *11*, 47. https://doi.org/10.1021/acsami.9b13259.

(21) Roose, B.; Dey, K.; Chiang, Y. H.; Friend, R. H.; Stranks, S. D. Critical Assessment of the Use of Excess Lead Iodide in Lead Halide Perovskite Solar Cells. *J. Phys. Chem. Lett.* **2020**, *11* (16), 6505–6512. https://doi.org/10.1021/acs.jpclett.0c01820.

(22) Kuang, Y.; Zardetto, V.; Van Gils, R.; Karwal, S.; Koushik, D.; Verheijen, M. A.; Black, L. E.; Weijtens, C.; Veenstra, S.; Andriessen, R.; et al. Low-Temperature Plasma-Assisted Atomic-Layer-Deposited SnO2as an Electron Transport Layer in Planar Perovskite Solar

Cells. *ACS Appl. Mater. Interfaces* **2018**, *10* (36), 30367–30378. https://doi.org/10.1021/acsami.8b09515.

(23) Wang, H.; Wang, Z.; Yang, Z.; Xu, Y.; Ding, Y.; Tan, L.; Yi, C.; Zhang, Z.; Meng, K.; Chen, G.; et al. Ligand-Modulated Excess PbI2 Nanosheets for Highly Efficient and Stable Perovskite Solar Cells. *Adv. Mater.* **2020**, *32* (21), 1–8. https://doi.org/10.1002/adma.202000865.

(24) Hu, Z.; An, Q.; Xiang, H.; Aigouy, L.; Sun, B.; Vaynzof, Y.; Chen, Z. Enhancing the Efficiency and Stability of Triple-Cation Perovskite Solar Cells by Eliminating Excess PbI2from the Perovskite/Hole Transport Layer Interface. *ACS Appl. Mater. Interfaces* **2020**, *12* (49), 54824–54832. https://doi.org/10.1021/acsami.0c17258.

(25) Xie, L. Q.; Chen, L.; Nan, Z. A.; Lin, H. X.; Wang, T.; Zhan, D. P.; Yan, J. W.; Mao, B. W.; Tian, Z. Q. Understanding the Cubic Phase Stabilization and Crystallization Kinetics in Mixed Cations and Halides Perovskite Single Crystals. *J. Am. Chem. Soc.* **2017**, *139* (9), 3320–3323. https://doi.org/10.1021/JACS.6B12432/SUPPL_FILE/JA6B12432_SI_002.CIF.

(26) Sun, Y.; Peng, J.; Chen, Y.; Yao, Y.; Liang, Z. Triple-Cation Mixed-Halide Perovskites: Towards Efficient, Annealing-Free and Air-Stable Solar Cells Enabled by Pb(SCN)2 Additive. *Sci. Reports 2017 71* **2017**, *7* (1), 1–7. https://doi.org/10.1038/srep46193.

(27) Chen, S.; Pan, L.; Ye, T.; Lei, N.; Yang, Y.; Wang, X. The Lattice Reconstruction of Cs-Introduced FAPbI 1.80 Br 1.20 Enables Improved Stability for Perovskite Solar Cells. *RSC Adv.* **2021**, *11* (7), 3997–4005. https://doi.org/10.1039/D0RA09294K.

(28) Zhou, N.; Shen, Y.; Zhang, Y.; Xu, Z.; Zheng, G.; Li, L.; Chen, Q.; Zhou, H. CsI Pre-Intercalation in the Inorganic Framework for Efficient and Stable FA1−x CsxPbI3(Cl) Perovskite Solar Cells. *Small* **2017**, *13* (23), 1700484. https://doi.org/10.1002/SMLL.201700484.

(29) Belarbi, E.; Vallés-Pelarda, M.; Clasen Hames, B.; Sanchez, R. S.; Barea, E. M.; Maghraoui-Meherzi, H.; Mora-Seró, I. Transformation of PbI2, PbBr2 and PbCl2 Salts into MAPbBr3 Perovskite by Halide Exchange as an Effective Method for Recombination Reduction. *Phys. Chem. Chem. Phys.* **2017**, *19* (17), 10913–10921. https://doi.org/10.1039/c7cp01192j.

(30) Condeles, J. F.; Lofrano, R. C. Z.; Rosolen, J. M.; Mulato, M. Stoichiometry, Surface and Structural Characterization of Lead Iodide Thin Films. *Brazilian J. Phys.* **2006**, *36* (2 A), 320–323. https://doi.org/10.1590/S0103-97332006000300023.

(31) Condeles, J. F.; Ando, R. A.; Mulato, M. Optical and Structural Properties of PbI2 Thin Films. *J. Mater. Sci.* **2008**, *43* (2), 525–529. https://doi.org/10.1007/S10853-007-1854-9/FIGURES/6.

(32) NIST X-Ray Photoelectron Database, Version 4.1, National Institute of Standards and Technology, Gaithersburg, 2012 https://srdata.nist.gov/xps/faq.aspx (accessed Nov 22, 2021).

(33) McGettrick, J. D.; Hooper, K.; Pockett, A.; Baker, J.; Troughton, J.; Carnie, M.; Watson, T. Sources of Pb(0) Artefacts during XPS Analysis of Lead Halide Perovskites. *Mater. Lett.* **2019**, *251*, 98–101. https://doi.org/10.1016/j.matlet.2019.04.081.

(34) Plekhanov, V. G. Lead Halides: Electronic Properties and Applications. *Prog. Mater. Sci.* **2004**, *49* (6), 787–886. https://doi.org/10.1016/S0079-6425(03)00049-5.

(35) Yuan, Y.; Xu, R.; Xu, H. T.; Hong, F.; Xu, F.; Wang, L. J. Nature of the Band Gap of Halide Perovskites ABX3 (A = CH3NH3, Cs; B = Sn, Pb; X = Cl, Br, I): First-Principles Calculations. *Chinese Phys. B* **2015**, *24* (11), 116302. https://doi.org/10.1088/1674-1056/24/11/116302.